This document is the Accepted Manuscript version of a Published Work that appeared in final form in Journal of Catalysis 327 (2015) 58–64. http://dx.doi.org/10.1016/j.jcat.2015.04.016.

Unraveling the structure sensitivity in methanol conversion on CeO_2: A DFT + *U* study

Marçal Capdevila-Cortada [a,*], Max García-Melchor [a,b], Núria López [a,*]

[a] *Institute of Chemical Research of Catalonia (ICIQ), Av. Països Catalans, 16, 43007 Tarragona, Spain*
[b] *SUNCAT Center for Interface Science and Catalysis, SLAC National Accelerator Laboratory, Menlo Park, CA 94025, USA*

A B S T R A C T

Methanol decomposes on oxides, in particular CeO_2, producing either formaldehyde or CO as main products. This reaction presents structure sensitivity to the point that the major product obtained depends on the facet exposed in the ceria nanostructures. Our density functional theory (DFT) calculations illustrate how the control of the surface facet and its inherent stoichiometry determine the sole formation of formaldehyde on the closed surfaces or the more degraded by-products on the open facets (CO and hydrogen). In addition, we found that the regular (100) termination is the only one that allows hydrogen evolution via a hydride–hydroxyl precursor. The fundamental insights presented for the differential catalytic reactivity of the different facets agree with the structure sensitivity found for ceria catalysts in several reactions and provide a better understanding on the need of shape control in selective processes.

Keywords:
CeO_2
Structure sensitivity
Methanol oxidation
Formaldehyde oxidation
Dehydrogenation
H_2 formation
DFT
Reaction mechanisms

1. Introduction

Cerium oxide, CeO_2, is a versatile and economically attractive oxide used in solid oxide fuel cells [1], biomedicine [2], and catalysis [3]. Either as a catalyst or as a support, it is widely used in a vast number of oxygen-related reactions such as the water–gas shift (WGS) [4,5], the preferential oxidation of CO [6,7], SO_2 oxidation [8,9], and the HCl conversion to Cl_2 [10]. All these applications are due to the particular redox character of ceria that permits to cycle between the Ce^{4+} and Ce^{3+} states, which involves oxygen vacancy formation [11] and diffusion [10,12]. The oxygen storage capacity (OSC) of CeO_2 varies with the exposing surface [13], and hence, in nanoparticles it ultimately depends on their morphology.

Recently, ceria has been also shown to present a high activity and selectivity in hydrogenation processes [10,14]. More surprisingly, the oxidation and hydrogenation capacities of different nanostructured CeO_2 materials have been found to present a markedly structure sensitivity [15]. Thus, while hydrogenation takes place preferentially on (111) facet orientations, oxidation reactions are favored on the more open (110) and (100) facets exposed in rods and cubes, respectively. Ceria nanoparticles have also been found to exhibit different activities in soot combustion depending on the exposed facet [16].

Among oxidation processes, the conversion of methanol to formaldehyde is considered an ideal test for characterizing the catalytic behavior of metal oxides [17,18]. The two main by-products of this reaction are water and hydrogen. Therefore, the catalytic activity and selectivity of a given material may be a result of the interplay between its oxidation and hydrogenation abilities.

In industry, methanol is oxidized to produce formaldehyde through the so-called Formox process [19]. There, methanol and oxygen react at temperatures around 525–675 K in the presence of iron oxide mixed with molybdenum or vanadium oxide according to the following equations:

$$CH_3OH + 1/2O_2 \rightarrow HCHO + H_2O \quad (1)$$

$$CH_3OH \rightarrow HCHO + H_2 \quad (2)$$

At higher temperatures, 875 K, silver can also act as catalyst, probably in the form of a suboxide [20–22]. Hence, the oxidation of methanol to formaldehyde has been extensively studied on metal oxides, especially on titanium and vanadium oxides [23–28]. In the case of ceria, most of the investigations have been focused on the (111) facet [29–33]. On this stoichiometric surface, methanol converts into formaldehyde, at *ca.* 550 K, via a dehydrogenation process that involves surface oxygens followed by the

* Corresponding authors.
E-mail addresses: mcapdevila@iciq.es (M. Capdevila-Cortada), nlopez@iciq.es (N. López).

subsequent reduction of two Ce^{4+} ions per methanol molecule [29]. The presence of oxygen vacancies was recently reported to have a detrimental effect on the reaction selectivity as a result of the competition between formaldehyde desorption and its further oxidation to CO [34]. In the same work, the (100) surface was also shown to have a reduced selectivity toward formaldehyde. Both HCHO and CO were found to be the main products on CeO_2(100), while on the reduced CeO_x(100) almost all methanol was converted to CO [34]. Temperature-programmed desorption (TPD) experiments on nanocrystals with different nanoshapes, namely octahedra, cubes, and rods, showed that the latter is the most reactive shape (but non-selective to formaldehyde) one, evolving CO and H_2 at $T < 583$ K [35]. On the other hand, Zhou and Mullins reported that formaldehyde does not decompose on stoichiometric CeO_2(111), but does evolve to CO and H_2 on the same reduced surface at temperatures above 500 K [36]. Overall, ceria appears to be very sensitive to the particular choice of active surfaces.

Despite all the above and other theoretical works reported in the literature [37–42], up to date there is no complete study assessing the selectivity of methanol dehydrogenation on the most representative ceria facets and proving their different behavior as experimentally observed. Herein, we present a thorough mechanistic study on the selective conversion of methanol to formaldehyde and its subsequent conversion to CO. To account for the particular morphology of the three common nanoshapes above, we have studied the three lowest index and energy surfaces (111), (110), and (100) (Fig. 1), as these are the most exposed facets in each nanoshape, respectively. The desorption of HCHO, CO, and H_2 from each surface is also discussed and compared to the reported TPD results on the stoichiometric ceria surfaces [29,33,34]. Overall, this work provides the clues behind the structure sensitivity in the aforementioned oxidation process.

2. Computational details

All the calculations reported in the present study were performed at the DFT + *U* level using the Vienna *Ab initio* Simulation Package (VASP, version 5.3.3) [43,44]. The Perdew–Becke–Ernzerhof (PBE) [45] functional was used in combination with an effective *U* term, U_{eff}, of 4.5 eV (this term is defined as the difference between the Coulomb, *U*, and the exchange, *J*, terms) [46], as it has been previously proven to provide satisfactory results [47–50]. The purpose of adding this Hubbard term *U* is to diminish the self-interaction error and to properly localize the Ce 4*f* states. Projector-augmented wave (PAW) pseudopotentials [51] were used to describe the core electrons with a plane-wave cutoff energy of 500 eV for the valence electrons (*i.e.*, 5*s*, 5*p*, 4*f*, 6*s* for Ce atoms, and 2*s*, 2*p*, for O and C atoms).

Ceria presents a fluorite structure, with lattice parameter a_{exp} = 5.411 Å [52]. We optimized the lattice parameter using a dense Γ-centered $7 \times 7 \times 7$ *k*-point mesh, leading to the value a_{calc} = 5.497 Å, in good agreement with both the experimental value and previous computational studies [53]. To maintain the stoichiometry of the CeO_2(100) surface and avoid the dipole moment normal to the surface, a half oxygen monolayer was transferred from the surface to the bottom of the slab [54]. The (111), (110), and (100) surfaces were modeled as (2×2) periodically repeated slabs consisting of four, five, and three O–Ce–O layers, respectively, separated by 15 Å of vacuum space, and were optimized using a Γ-centered *k*-point mesh denser than 0.38 $Å^{-1}$. The layers allowed to relax in each surface were the five outermost layers in CeO_2(111), the three top-most layers in CeO_2(110), and the four outermost layers in CeO_2(100), whereas the rest of atoms were kept fixed to their bulk positions.

Transition states were located by means of the climbing image nudged elastic band (CI-NEB) method [55]. The nature of all reaction minima and transition states was confirmed by means of numerical frequency analyses.

3. Results

3.1. Dehydrogenation of methanol to formaldehyde on CeO_2

We investigated the conversion of methanol to formaldehyde on the three lowest energy surfaces corresponding to the low-index planes (111), (110), and (100). Their surface and relaxation energies are presented in the Supplementary Material (Table S1).

The reaction consists in the sequence of the following elementary steps:

$$CH_3OH + {}^* \rightarrow CH_3OH^* \quad (R1)$$

$$CH_3OH^* + {}^* \rightarrow CH_3O^* + H^* \quad (R2)$$

$$CH_3O^* + {}^* \rightarrow HCHO^* + H^* \quad (R3)$$

$$HCHO^* \rightarrow HCHO + {}^* \quad (R4)$$

Methanol physisorbs on ceria (R1) and dissociates (R2) giving rise to a chemisorbed methoxy and surface OH groups. The methoxy intermediate then leads to formaldehyde through a C–H bond breaking (R3) with the concomitant hydrogenation of another surface oxygen. Finally, formaldehyde desorbs from the surface to the gas phase (R4).

Reaction (R2) is controlled by the acid–base properties of the surface and does not involve any change in the oxidation state of the reactant fragments or the surface metal atoms. In contrast, reaction (R3) can be seen as the main redox step as two Ce^{4+} cations are reduced to Ce^{3+} after the C–H scission and the subsequent formation of a second surface OH group. The discrimination in terms of acid–base and redox steps has been recently found to be crucial to tune the catalytic activity of oxides [56].

The calculated energy profiles for the methanol to formaldehyde conversion on the different CeO_2 surfaces are presented in

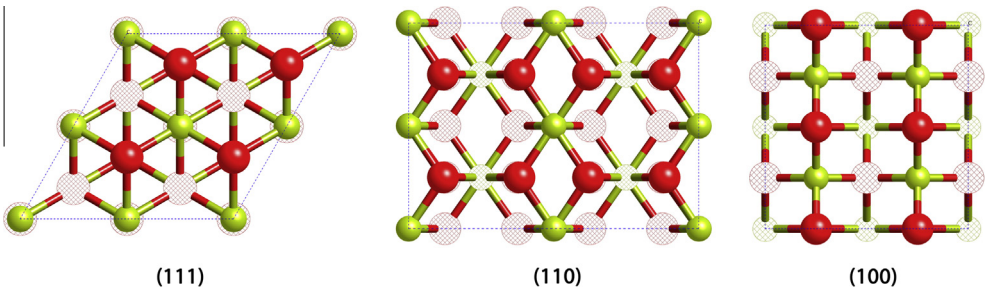

Fig. 1. Top views of the three lowest index CeO_2 surfaces. The outmost oxygen (in red) and cerium (in green) layers are highlighted, while the rest of atoms are shown dashed. (For interpretation of the references to color in this figure legend, the reader is referred to the web version of this article.)

Fig. 2. Methanol adsorption energies range between −0.5 and −1 eV, whereas the first deprotonation requires very low energies, <0.1 eV, rendering a more stable methoxy intermediate (**I1**). From this point, the relative energy barrier for the next step (R3) on all the surfaces is around 1 eV. More specifically, the (100) surface exhibits the lowest energy barrier (0.89 eV), whereas the (111) and (110) surfaces have barriers of 1.03 and 1.14 eV, respectively. In all the cases, the transition state associated with this process (**TS2**) involves the reduction of one single Ce^{4+} to Ce^{3+}, whereas the other unpaired electron resulting from the C–H scission is delocalized over these C and H atoms and the involved surface oxygen. On the (111) surface, the C–H scission in **I1** results in the physisorbed formaldehyde as intermediate, as also noted by Kropp and Paier [39]. The next barrier from the physisorbed to chemisorbed conformation (**I2**) is lower than 0.05 eV (see Supplementary Material Fig. S2). Alternatively, on the (110), the C–H bond cleavage leads to the formation of an intermediate where HCHO is directly chemisorbed on the hydroxylated surface group. From this species, the following proton transfer to the adjacent surface oxygen leading to **I2** only requires 0.02 eV. Importantly, the energy barrier for the direct formation of **I2** from **I1** on the (110) was previously reported [38] as 0.9 eV higher than ours. We found that the direct mechanism from **I1** to **I2** via the transition state **TS2** is only favored on the (100) surface.

In **I2**, formaldehyde binds to the surface in a η_2-like configuration, where the C atom is coordinated to an oxygen from the lattice and the oxygen from HCHO is bound to a surface cation. This species is rather stable on all the surfaces, with binding energies of 1.23, 0.71, and 2.30 eV for the (111), (110), and (100) facets, respectively. Hence, formaldehyde desorption from the (111) and (110) surfaces is expected to be significantly easier compared to (100). That is, the lifetime of HCHO on the (100) surface may be higher than on the other surfaces, which might eventually lead to surface poisoning.

Overall, according to the energy diagram in Fig. 2, the most energy-demanding step in the methanol to formaldehyde conversion on the (110) surface is the C–H bond breaking, whereas on the (100) and (111) surfaces it corresponds to formaldehyde desorption.

3.2. Dehydrogenation of formaldehyde to carbon monoxide on CeO_2

The reaction mechanism for the dehydrogenation of formaldehyde to CO on the clean (111), (110), and (100) surfaces was analyzed assuming the following elementary reaction steps:

$$HCHO + {}^* \rightarrow HCHO^* \quad (R4')$$

$$HCHO^* + {}^* \rightarrow CHO^* + H^* \quad (R5)$$

$$CHO^* + {}^* \rightarrow CO^* + H^* \quad (R6)$$

$$CO^* \rightarrow CO + {}^* \quad (R7)$$

In this case, the initial step (R4′) is the reverse process of the above (R4) reaction. After the adsorption of formaldehyde, the reaction then proceeds through two consecutive H abstractions

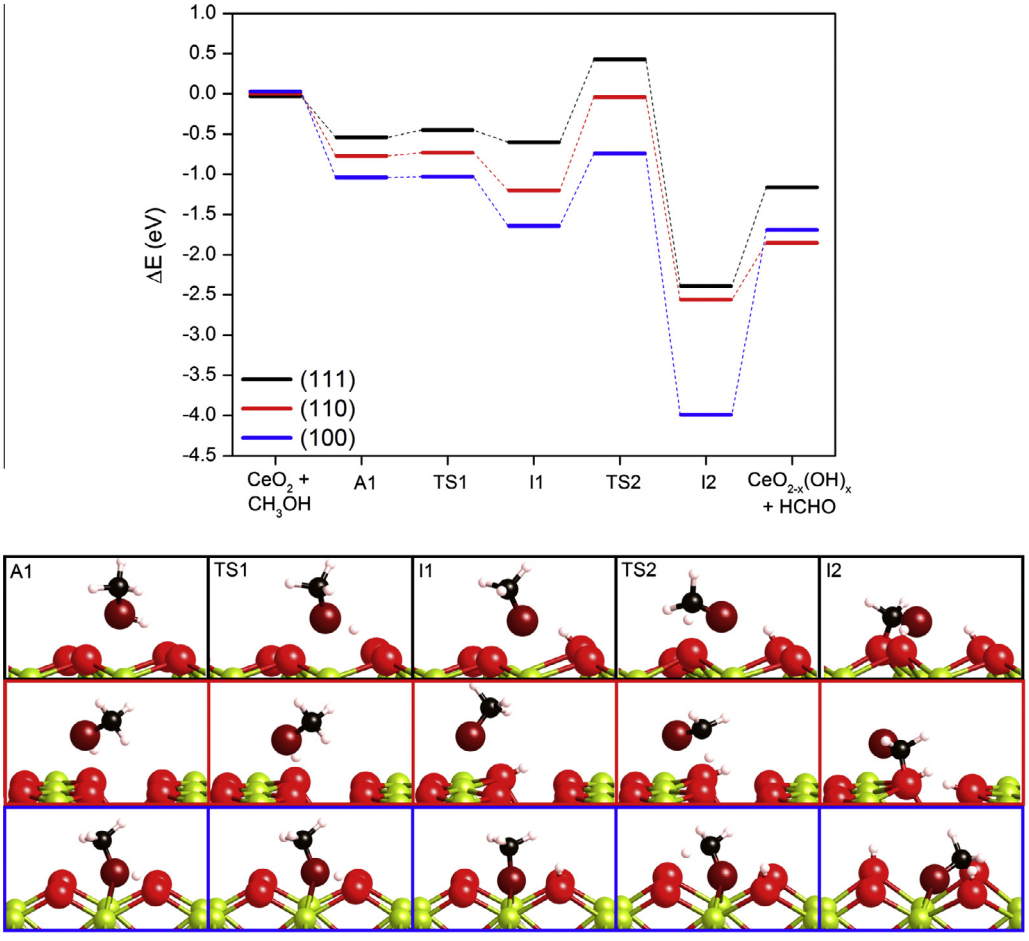

Fig. 2. Top panel: energy profile for the MeOH to HCHO conversion on CeO_2(111), CeO_2(110), and CeO_2(100). Bottom panel: optimized geometries for the intermediates and transition states. The most relevant distances in the transition states can be found in Fig. S1. Color code as in Fig. 1 with the addition of C (black), O from methanol (dark red), and H (white). (For interpretation of the references to color in this figure legend, the reader is referred to the web version of this article.)

(R5) and (R6), which can be again considered as coupled redox and acid–base steps. Finally, the generated CO desorbs from the surface to the gas phase. The reaction energy profiles obtained for the three CeO_2 surfaces are shown in Fig. 3. The initial formaldehyde chemisorption value (**A2**) on the (111), (110), and (100) surfaces is −0.88, −1.25, and −1.84 eV, respectively. Note that the lower binding energies for the (111) and (100) facets compared to **I2** in the methanol dehydrogenation (Fig. 2) are due to the formation of hydrogen bonds between HCHO and the surface hydroxyls [57]. The energy difference can be estimated to the formation of two hydrogen bonds [58]. On (110), **A2** binding energy is higher than **I2** because the hydroxylated surface presents intrasurface hydrogen bonds (between O_{lat}–H and another O_{lat}) and formaldehyde adsorbs on the acceptor oxygen disrupting the H-bond surface network. From **A2**, the first H abstraction in HCHO is a highly exothermic process that releases more than -2 eV and results in the chemisorbed formyl and one surface hydroxyl group (**I3**). The activation energy for this step requires only 0.66 eV on the (100) surface, but is very energy demanding on both (111) and (110), that is, 1.53 and 1.87 eV, respectively. Similar to the H stripping in methanol (R3), in this first transition state (**TS3**), one Ce^{4+} is reduced to Ce^{3+}, while the other unpaired electron is delocalized over the formaldehyde and the reacting surface oxygen. The second deprotonation step (R6) is endothermic and produces physisorbed CO and two surface OH groups. The energy barriers for this step on the (111) and (100) surfaces are 1.60 and 1.64 eV, respectively, and 2.00 eV on the (110). Finally, the CO desorption from the partially hydroxylated surfaces requires only 0.1–0.3 eV. It is worth noting that CO can also form a carbonate structure CO_3^{2-} with two surface oxygens. This structure is 3.5 eV more stable than the physisorbed CO [59,60], although its formation requires two accessible surface oxygens. On hydroxylated surfaces, HCO_3^- and H_2CO_3 could be formed, which are 1.8 eV more stable and 1.3 eV less stable, respectively, than physisorbed CO. Therefore, highly hydroxylated surfaces are less prone to form carbonates, and their formation (HCO_3^- and H_2CO_3) would not introduce significant alterations to the proposed mechanism.

Alternatively, the oxidation of the chemisorbed formaldehyde on the (100) surface can also follow the blue dashed path shown in Fig. 3. In this case, the H atom resulting from the first C–H scission accommodates between two surface Ce^{4+} cations as a hydride. Thus, unlike the previous mechanism, this alternative pathway does not involve the reduction of any surface cerium cations [61]. This first H abstraction is endothermic by 0.66 eV and requires an activation energy of 0.75 eV. Similarly, the subsequent C–H bond cleavage is also endothermic by 1.06 eV and

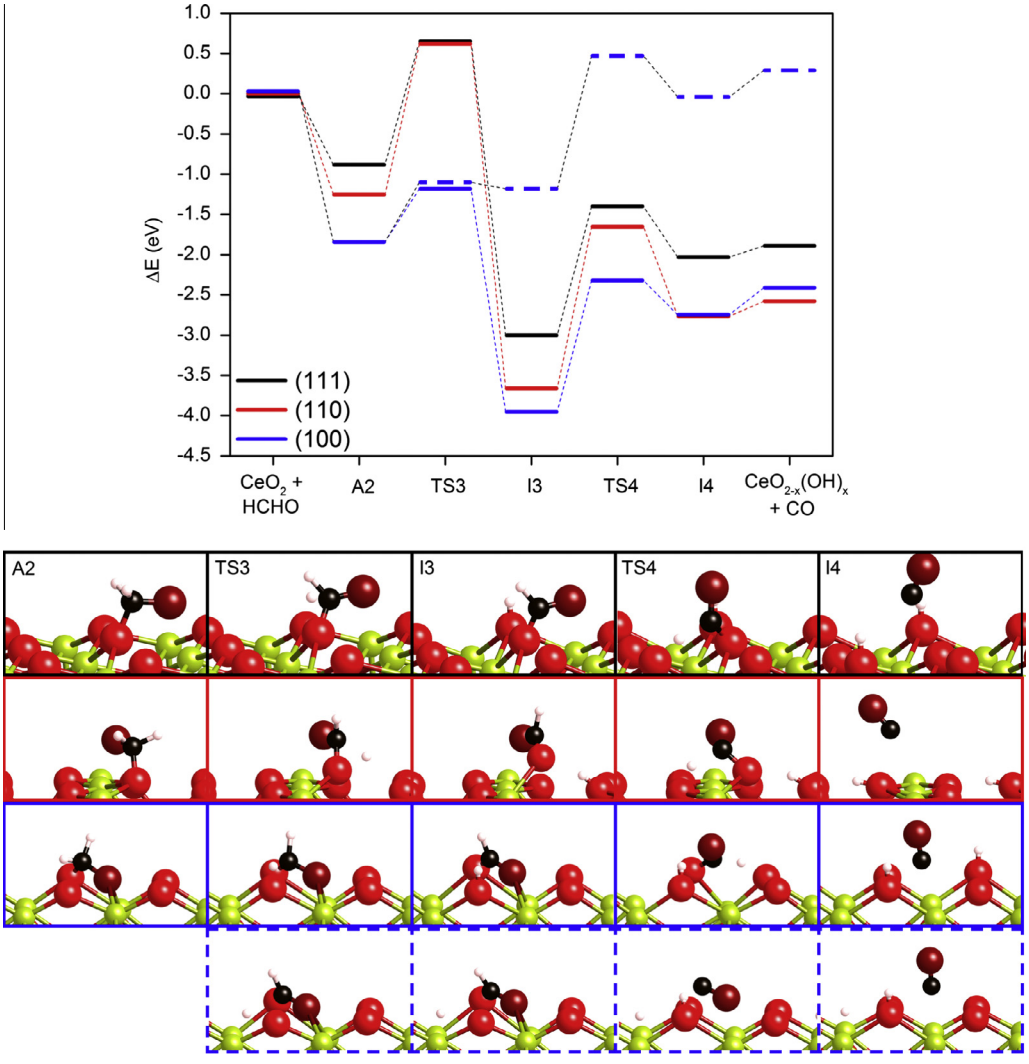

Fig. 3. Top panel: energy profile for the HCHO conversion to CO upon adsorption on CeO_2(111), CeO_2(110), and CeO_2(100). The alternative hydride cleavage mechanism on the latter surface is shown in dashed blue lines. Bottom panel: optimized geometries for the intermediates and transition states. The most relevant distances in the transition states can be found in Fig. S3. Color code as in Fig. 2. (For interpretation of the references to color in this figure legend, the reader is referred to the web version of this article.)

has an energy barrier of 1.82 eV. Although this alternative mechanism is thermodynamically less favored than the previous one (solid lines in Fig. 3), it might play a role under high coverage regimes, where all surface oxygens would be poisoned by chemisorbed formaldehyde. It is worth mentioning that this mechanism is enabled only on the particularly defective (100) surface, and is unlikely to occur on the other two surfaces (Fig. S4).

On the whole, Fig. 3 shows that the most energy-demanding step for the oxidation of formaldehyde to CO is the same for the three ceria facets and corresponds to the cleavage of the second C–H bond (R6). The activation energies for the (R5) and (R6) steps range between 1.5 and 2 eV, except for (R5) on the (100), which is only 0.66 eV. On (111) and (110), the energies required to reach **TS3** are ca. 0.6 eV higher than the desorption of formaldehyde from these surfaces.

3.3. H_2 evolution from a hydroxylated CeO_2 surface

Once methanol decomposes to either HCHO or CO, the CeO_2 surfaces become partially hydroxylated, which can eventually lead to hydrogen evolution under certain reaction conditions. In a previous work, we showed that H_2 dissociation on the (111) surface affords the homolytic product although through an heterolytic path involving the formation of an ion pair as precursor [50]. The reaction profile for that reverse process on the three CeO_2 surfaces is presented in Fig. 4. In the first step, one hydrogen of the two surface hydroxyl groups is transferred to a neighboring cerium atom with the concomitant oxidation of one Ce^{3+} to Ce^{4+}. This process is highly endothermic, the reaction energies being 3.22 eV on (111), 3.61 eV on the (110), and 2.71 eV on the (100), and the associated barriers 3.55, 4.30, and 3.53 eV, respectively. Interestingly, the resulting product **I5** features a completely different nature depending on the considered facet, see Fig. 4. While on the (111) and (110) surfaces, it can be described as an ion pair with a H–H distance of 1.29 and 1.65 Å, respectively, on the (100) surface, this ion pair is not stable and the proton and the hydride fall apart so that the latter accommodates between two Ce^{4+}. This is a consequence of the intrinsic oxygen depletion of the (100) surface. These significant structural differences are also reflected in substantially different stabilities. More specifically, the ion pairs formed on the (111) and (110) surfaces have energies of 0.75 and 0.45 eV above the gas-phase reference, respectively, whereas the charge separated form on (100) is −0.29 eV more stable. From these precursors, the activation energy for the following H–H bond formation on (111) and (110) is very low, 0.1 eV, but it increases to 0.62 eV on the (100).

Thus, hydrogen evolution on the (111) and (110) surfaces is very difficult as H is always stored as hydroxyl on the regular stoichiometric surfaces. In contrast, as mentioned above, the situation on the (100) surface might be different. In fact, when methanol is adsorbed on this surface, a large coverage of hydroxyls is likely; therefore, the hydrogen stripping from **A2** can divert toward the production of the intermediate **I3** (dashed blue line mechanism), where one of the hydrogens is transferred as a hydride. This situation is equivalent to that presented in structure **I5**, from which we have shown that H_2 can be evolved with a small energy barrier.

The evolution of hydrogen from the hydroxylated surface might also compete with the formation of water and its subsequent desorption, thus creating an oxygen vacancy. This overall process is endothermic on all three surfaces, by 2.22, 2.11, and 2.34 eV on (111), (110), and (100), respectively. Despite being a highly endothermic process, it is more likely to occur than the hydrogen evolution from the hydroxylated surface.

4. Discussion

In this section, we present a detailed comparison between our DFT simulations and the available experiments in the literature. The theoretical results exposed in the previous sections are perfectly consistent with the reported TPD experiments on stoichiometric (111) and (100) CeO_2 thin films [29,33,34]. In the case of the (111) surface, the only desorption products observed are formaldehyde and methanol. Methanol desorbs at 220 K (main peak) and 560 K, and formaldehyde at 570 K. Similarly, TPD experiments on the (100) surface show the same product distribution but with the additional observation of CO, CO_2, H_2O, and H_2. In this case, methanol appears at 560–580 K, with a large peak of formaldehyde and CO coupled with a smaller peak assigned to H_2 and H_2O. Moreover, the reaction on this surface was reported to occur rapidly and without detecting any formyl or formate intermediates. The desorption peaks for HCHO, CO, and H_2 for both the (111) and (100) facets proceed prior to any indication of surface reduction (related to CO_2 or H_2O desorption peaks).

The above structure sensitivity observed in experiments can be rationalized as follows on the basis of our theoretical calculations. Even though we showed that the sequential removal of H from methanol on the (111) and (110) surfaces is energetically costly, it derives on adsorbed formaldehyde, which can be desorbed more easily than the further removal of H from it. That is, the adsorption energy of **A2** in Fig. 3 is significantly smaller than the energy required to reach **TS3**. As a result, methanol selectively reacts toward formaldehyde on the (111) and (110) surfaces, the latter being more reactive (lower **TS2**) than the former. Major differences, however, can be found in reaction conversions. On the (111) surface, methanol desorption and its transformation to formaldehyde are competing processes, but the weak interaction between methanol and the surface results in a large peak in the TPD at low temperatures. Still, some methanol molecules survive on the surface long enough to react, possibly pinned by undersurface vacancies [62,63]. This is clearly evidenced in the TPD experiments where the low-temperature peak (methanol desorption) is larger than the others for the (111) surface under stoichiometric conditions. In contrast, on the (100) surface, the energy demand to reach **TS3** is much lower than the adsorption energy of **A2**, and therefore, the conversion of formaldehyde to CO is favored compared to formaldehyde desorption. These results also account for the unique experimental observation of CO on the most oxidized CeO_2(100) surfaces [34]. It was also shown that CO is more likely to appear on the more defective ceria surfaces. This can be also explained with the expected increase of the **A2** adsorption energy on the O-vacancy sites, as these may trap HCHO and impede its desorption, thus favoring CO evolution.

This is in fact the case for the (111) surface, where methanol adsorbs dissociatively on the defective site with an adsorption energy of −2.12 eV [64]. The subsequent C–H cleavage to form the chemisorbed formaldehyde demands 1.32 eV and is an exothermic process by 0.34 eV. Formaldehyde desorption from this surface requires 1.04 eV, and the energy barrier for the subsequent C–H bond breaking is only 0.58 eV. Hence, the oxygen deficiency (111) traps formaldehyde and enables methanol conversion to CO, as suggested before and shown in the reported TPD experiments [34].

When it comes to hydrogen, experiments show that only CeO_2(100) is able to evolve molecular hydrogen at about 600 K [34]. Indeed, from Fig. 4, it can be observed that the surface OH groups are too robust to produce H_2 from any of the three surfaces. However, on the (100), the intrinsic lack of surface oxygen makes the situation less compromised as both hydrides and protons can be stabilized by the surface Ce and O atoms. Hence, populating this

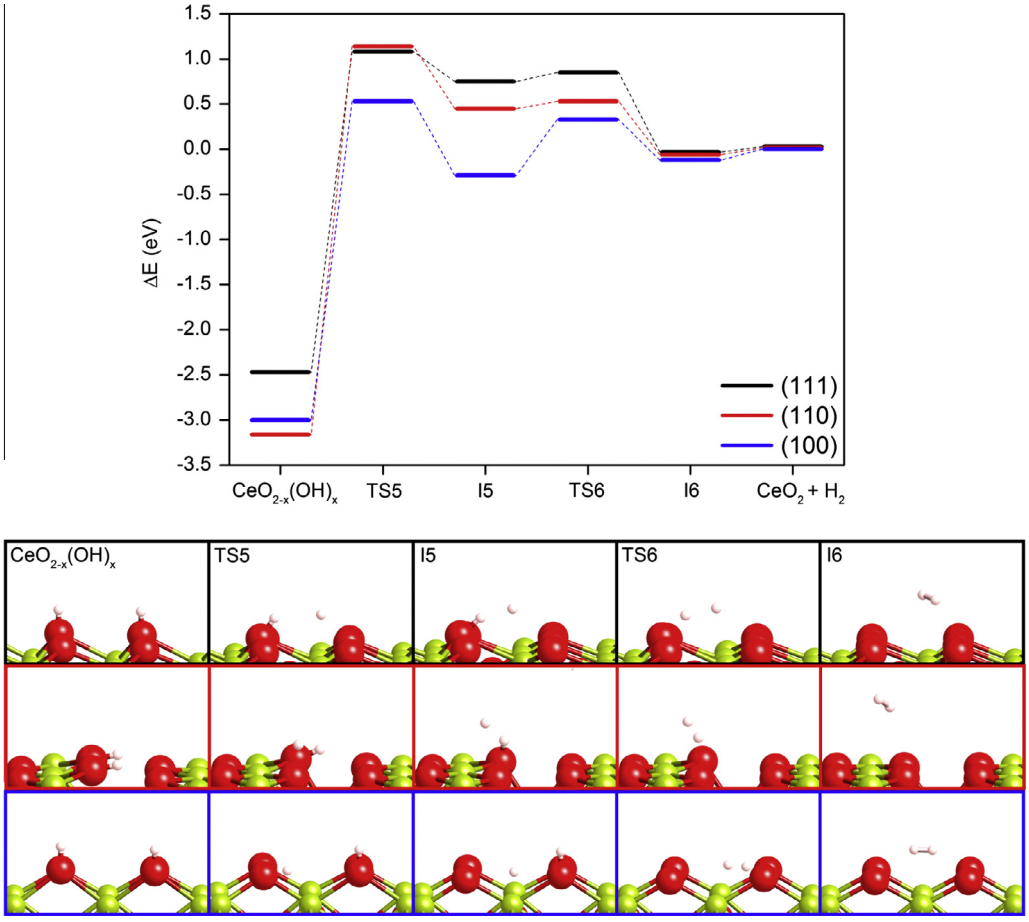

Fig. 4. Top panel: energy profile for H_2 evolution from partially hydroxylated (0.5 ML) CeO_2(111), CeO_2(110), and CeO_2(100). Bottom panel: optimized geometries for the intermediates and transition states. Color code as in Fig. 2. (For interpretation of the references to color in this figure legend, the reader is referred to the web version of this article.)

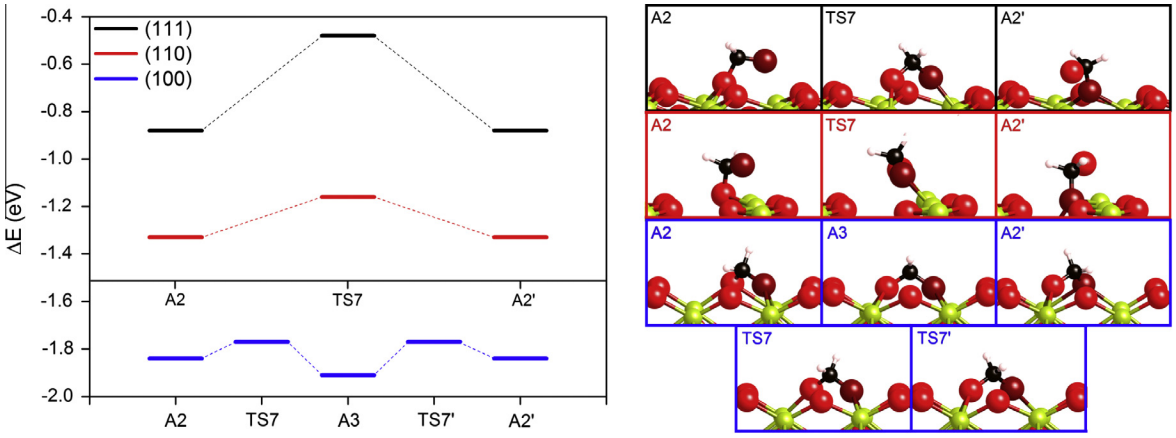

Fig. 5. Left: energy profile for the oxygen exchange between HCHO and a lattice oxygen from CeO_2(111), CeO_2(110), and CeO_2(100). Right: optimized geometries for the intermediates and transition states. Color codes as in Fig. 2. (For interpretation of the references to color in this figure legend, the reader is referred to the web version of this article.)

state is crucial for CeO_2 to be able to generate H_2. This also explains why H_2 evolution is also observed experimentally on defective CeO_2(111) surfaces [34]. Our results also point out that formaldehyde oxidation on the (100) surface can take place through a less thermodynamically favored alternative mechanism and without involving the reduction of surface Ce ions (blue dashed path in Fig. 3). Upon CO desorption, this reaction path leads to the partially hydroxylated surface **I5**, which might enhance H_2 evolution on the (100) surface, especially under high coverage regimes with all the surface oxygens occupied by chemisorbed formaldehyde. This mechanism, accessible for the intrinsically O-deficient (100) surface, also explains why reduced (111) surfaces can also produce H_2. These reduced surfaces can trap hydride atoms and follow a similar mechanism as the one we proposed for the (100) surface.

Finally, the reported TPD spectrum using isotope-labeled ceria and methanol, $Ce^{18}O_2$(111) and $CH_3^{16}OH$, shows that an equal

amount of $HCH^{16}O$ and $HCH^{18}O$ is desorbed [29]. The same observation is made upon $HCH^{16}O$ adsorption on reduced $Ce^{18}O_{1.75}(111)$ [36]. The latter was attributed by the authors to the adsorption on a vacancy site.

In order to shed light on these experimental findings, we also investigated a reaction mechanism in which an O atom from the chemisorbed HCHO is exchanged with one lattice oxygen from the stoichiometric CeO_2 surfaces (Fig. 5). On (111) and (110), this mechanism occurs in an elementary step with an activation energy of 0.40 and 0.17 eV. In contrast, on the (100) termination, the chemisorbed formaldehyde **A2** gives rise to an intermediate (**A3**) that is 0.07 eV more stable and where the lattice oxygen has diffused and accommodates on a defective surface site. The energy barrier required to afford **A3** is also very low (0.08 eV). The low energy difference and activation energy between both **A2** and **A3** indicate that these two intermediates may be in thermodynamic equilibrium. Therefore, the low activation energies found for this process on the different CeO_2 surfaces prove that no oxygen vacancies are needed to desorb $HCH^{18}O$ upon $HCH^{16}O$ adsorption or $CH_3^{16}OH$ dehydrogenation.

5. Conclusions

A detailed mechanistic study on the reported structure sensitivity of different CeO_2 surfaces in the methanol conversion to formaldehyde or *syn*-gas ($CO + H_2$ mixtures) has been performed. The reaction proceeds via the activation of the hydroxyl group by the basic sites on the surface and followed by the subsequent stripping of hydrogen atoms from the methyl group. Our DFT + *U* calculations show that while close-packed surfaces mainly produce formaldehyde, this intermediate is trapped in the O-defective (100) surface, which finally produces CO and H_2. Hydrogen evolution is allowed on the (100) facet, but not on the close-packed (111) and (110) terminations. This is due to the inherent defective sites in the former that stabilize two hydrogen atoms as hydroxyls and hydrides, which eventually lead to H–H bond formation. Only reduced (111) and (110) surfaces could present enough vacancy sites to allow a similar chemistry on the close-packed facets. These active sites in turn extend the lifetime of adsorbed HCHO enabling its decomposition, and are ultimate responsible for CO formation.

The present work sheds light on the structure sensitivity found for the reaction and that is related to the inherent stoichiometries of the different surfaces. This is more acute on oxides, in particular reducible ones, as there are more parameters that are modified when changing the facet orientations. Moreover, shape control is a key to obtain desired selectivities, and thus, methods devoted to a detailed shape selection are crucial to obtain a more selective and greener chemistry.

Acknowledgments

This research has been supported by the ERC Starting Grant (ERC-2010-StG-258406). We acknowledge BSC-RES for providing generous computational resources.

Appendix A. Supplementary material

Supplementary data associated with this article can be found, in the online version, at http://dx.doi.org/10.1016/j.jcat.2015.04.016.

References

[1] Z. Shao, S.M. Haile, Nature 431 (2004) 170.
[2] A.S. Karakoti, S. Singh, A. Kumar, M. Malinska, S.V.N.T. Kuchibhatla, K. Wozniak, et al., J. Am. Chem. Soc. 131 (2009) 14144.
[3] A. Trovarelli, Catalysis by Ceria and Related Materials, Imperial College Press, London, 2002.
[4] Q. Fu, H. Saltsburg, M. Flytzani-Stephanopoulos, Science 301 (2003) 935.
[5] S. Hilaire, X. Wang, T. Luo, R. Gorte, J. Wagner, Appl. Catal. A Gen. 215 (2001) 271.
[6] M.M. Schubert, V. Plzak, J. Garche, R.J. Behm, Catal. Lett. 76 (2001) 143.
[7] O. Pozdnyakova, D. Teschner, A. Wootsch, J. Kröhnert, B. Steinhauer, H. Sauer, et al., J. Catal. 237 (2006) 1.
[8] J.S. Yoo, A.A. Bhattacharyya, C.A. Radlowski, Ind. Eng. Chem. Res. 30 (1991) 1444.
[9] J.S. Yoo, A.A. Bhattacharyya, C.A. Radlowski, J.A. Karch, Appl. Catal. B Environ. 1 (1992) 169.
[10] A.P. Amrute, C. Mondelli, M. Moser, G. Novell-Leruth, N. López, D. Rosenthal, et al., J. Catal. 286 (2012) 287.
[11] M. Nolan, S.C. Parker, G.W. Watson, Surf. Sci. 595 (2005) 223.
[12] D.A. Andersson, S.I. Simak, N.V. Skorodumova, I.A. Abrikosov, B. Johansson, Proc. Natl. Acad. Sci. USA 103 (2006) 3518.
[13] J. Paier, C. Penschke, J. Sauer, Chem. Rev. 113 (2013) 3949.
[14] G. Vilé, B. Bridier, J. Wichert, J. Pérez-Ramírez, Angew. Chem. Int. Ed. 51 (2012) 8620.
[15] G. Vilé, S. Colussi, F. Krumeich, A. Trovarelli, J. Pérez-Ramírez, Angew. Chem. Int. Ed. 53 (2014) 12069.
[16] E. Aneggi, D. Wiater, C. de Leitenburg, J. Llorca, A. Trovarelli, ACS Catal. 4 (2014) 172.
[17] J.M. Tatibouët, Appl. Catal. A Gen. 148 (1997) 213.
[18] M. Badlani, I.E. Wachs, Catal. Lett. 75 (2001) 137.
[19] http://www.formox.com/, November 2014.
[20] M. Schmid, A. Reicho, A. Stierle, I. Costina, J. Klikovits, P. Kostelnik, et al., Phys. Rev. Lett. 96 (2006) 146102.
[21] J. Schnadt, A. Michaelides, J. Knudsen, R. Vang, K. Reuter, E. Lægsgaard, et al., Phys. Rev. Lett. 96 (2006) 146101.
[22] I. Karakaya, W.T. Thompson, J. Phase Equilibria 13 (1992) 137.
[23] J.L. Bronkema, D.C. Leo, A.T. Bell, J. Phys. Chem. C. 111 (2007) 14530.
[24] L.J. Burcham, I.E. Wachs, Catal. Today 49 (1999) 467.
[25] G. Deo, I.E. Wachs, J. Catal. 146 (1994) 323.
[26] T. Feng, J.M. Vohs, J. Catal. 208 (2002) 301.
[27] Y. Romanyshyn, S. Guimond, H. Kuhlenbeck, S. Kaya, R.P. Blum, H. Niehus, et al., Top. Catal. 50 (2008) 106.
[28] Q. Wang, R.J. Madix, Surf. Sci. 496 (2002) 51.
[29] D.R. Mullins, M.D. Robbins, J. Zhou, Surf. Sci. 600 (2006) 1547.
[30] A. Siokou, R.M. Nix, J. Phys. Chem. B 103 (1999) 6984.
[31] J.J. Uhlrich, B. Yang, S. Shaikhutdinov, Top. Catal. 57 (2014) 1229.
[32] V. Matolín, J. Libra, M. Škoda, N. Tsud, K.C. Prince, T. Skála, Surf. Sci. 603 (2009) 1087.
[33] R.M. Ferrizz, G.S. Wong, T. Egami, J.M. Vohs, Langmuir 17 (2001) 2464.
[34] P.M. Albrecht, D.R. Mullins, Langmuir 29 (2013) 4559.
[35] Z. Wu, M. Li, D.R. Mullins, S.H. Overbury, ACS Catal. 2 (2012) 2224.
[36] J. Zhou, D.R. Mullins, Surf. Sci. 600 (2006) 1540.
[37] D. Mei, N.A. Deskins, M. Dupuis, Q. Ge, J. Phys. Chem. C 111 (2007) 10514.
[38] D. Mei, N.A. Deskins, M. Dupuis, Q. Ge, J. Phys. Chem. C 112 (2008) 4257.
[39] T. Kropp, J. Paier, J. Phys. Chem. C 118 (2014) 23690.
[40] M. Nolan, J. Chem. Phys. 139 (2013) 184710.
[41] T. Kropp, J. Paier, J. Sauer, J. Am. Chem. Soc. 136 (2014) 14616.
[42] B.-T. Teng, S.-Y. Jiang, Z.-X. Yang, M.-F. Luo, Y.-Z. Lan, Surf. Sci. 604 (2010) 68.
[43] G. Kresse, Phys. Rev. B 54 (1996) 11169.
[44] G. Kresse, J. Furthmüller, Comput. Mater. Sci. 6 (1996) 15.
[45] J.P. Perdew, K. Burke, M. Ernzerhof, Phys. Rev. Lett. 77 (1996) 3865.
[46] S.L. Dudarev, S.Y. Savrasov, C.J. Humphreys, A.P. Sutton, Phys. Rev. B 57 (1998) 1505.
[47] S. Fabris, S. de Gironcoli, S. Baroni, G. Vicario, G. Balducci, Phys. Rev. B 72 (2005) 237102.
[48] M. Ganduglia-Pirovano, J. Da Silva, J. Sauer, Phys. Rev. Lett. 102 (2009) 026101.
[49] R. Farra, M. García-Melchor, M. Eichelbaum, M. Hashagen, W. Frandsen, J. Allan, et al., ACS Catal. 3 (2013) 2256.
[50] M. García-Melchor, N. López, J. Phys. Chem. C 118 (2014) 10921.
[51] P.E. Blöchl, Phys. Rev. B 50 (1994) 17953.
[52] E. Kümmerle, G. Heger, J. Solid State Chem. 147 (1999) 485.
[53] J. Da Silva, M. Ganduglia-Pirovano, J. Sauer, V. Bayer, G. Kresse, Phys. Rev. B 75 (2007) 045121.
[54] P. Oliver, G. Watson, S. Parker, Phys. Rev. B 52 (1995) 5323.
[55] G. Henkelman, B.P. Uberuaga, H. Jónsson, J. Chem. Phys. 113 (2000) 9901.
[56] M. Moser, I. Czekaj, N. López, J. Pérez-Ramírez, Angew. Chem. Int. Ed. 53 (2014) 8628.
[57] D. Fernández-Torre, K. Kośmider, J. Carrasco, M.V. Ganduglia-Pirovano, R. Pérez, J. Phys. Chem. C 116 (2012) 13584.
[58] G. Revilla-López, N. López, Phys. Chem. Chem. Phys. 16 (2014) 18933.
[59] M. Nolan, G.W. Watson, J. Phys. Chem. B 110 (2006) 16600.
[60] M. Nolan, S.C. Parker, G.W. Watson, Surf. Sci. 600 (2006) 175.
[61] This fact was confirmed by the obtained spin densities at this surface.
[62] F. Esch, S. Fabris, L. Zhou, T. Montini, C. Africh, P. Fornasiero, et al., Science 309 (2005) 752.
[63] G.E. Murgida, M.V. Ganduglia-Pirovano, Phys. Rev. Lett. 110 (2013) 246101.
[64] Calculations on defective ceria (111) were performed using the p(2×2) model slab described in the Computational details section. Nevertheless, the results are in close agreement with those in Ref. [41].